Title

Analysis of the Role of the Conserved Disulfide in Amyloid Formation by Human Islet Amyloid Polypeptide in Homogeneous and Heterogeneous Environments

Journal

Biochemistry, 57(21)

ISSN

0006-2960

Authors

Ridgway, Zachary
Zhang, Xiaoxue
Wong, Amy G
et al.

Publication Date

2018-05-29

DOI

10.1021/acs.biochem.8b00017

Peer reviewed

HHS Public Access

Author manuscript

Biochemistry. Author manuscript; available in PMC 2019 May 29.

Published in final edited form as:

Biochemistry. 2018 May 29; 57(21): 3065–3074. doi:10.1021/acs.biochem.8b00017.

Analysis of the role of the conserved disulfide in amyloid formation by human IAPP in homogenous and heterogeneous environments

Zachary Ridgway[(1),‡], **Xiaoxue Zhang**[(1),‡], **Amy G. Wong**[(1)], **Andisheh Abedini**[(2)], **Ann Marie Schmidt**[(2)], and **Daniel P. Raleigh**[(1),(3),*]

[(1)]Department of Chemistry, Stony Brook University, Stony Brook, NY 11794-3400, USA

[(2)]Diabetes Research Program, Division of Endocrinology, Diabetes and Metabolism, Department of Medicine, New York University School of Medicine, New York, United States

[(3)]Laufer Center for Quantitative Biology, Stony Brook University Stony Brook, NY 11794-3400, USA

Abstract

Human islet amyloid polypeptide (hIAPP) is a hormone secreted from β-cells in the Islets of Langerhans in response to the same stimuli that lead to insulin secretion. hIAPP plays an adaptive role in glucose homeostasis, but misfolds to form insoluble, fibrillar aggregates in type-II diabetes that are associated with the disease. Along the misfolding pathway, hIAPP forms species that are toxic to β-cells, resulting in reduced β-cell mass. hIAPP contains a strictly conserved disulfide bond between residues 2–7, which forms a small loop at the N-terminus of the molecule. The loop is located outside of the cross β-core in all models of the hIAPP amyloid fibrils. Mutations in this region are rare, and the disulfide loop plays a role in receptor binding, but the contribution of this region to the aggregation of hIAPP is not well understood. We define the role of the disulfide by analyzing a collection of analogues that remove the disulfide, by mutation of Cys to Ser, by reduction and modification of the Cys residues, or by deletion of the first seven residues. The cytotoxic properties of hIAPP are retained in the Cys to Ser disulfide free mutant. Removal of the disulfide bond accelerates amyloid formation in all constructs, both in solution and in the presence of model membranes. Removal of the disulfide reduces the ability of hIAPP to induce leakage of vesicles made up of POPS and POPC. Smaller effects are observed with vesicles that contain 40 mole percent cholesterol, although N-terminal truncation still reduces leakage.

Graphical Abstract

[*]Author to whom correspondence should be addressed: Daniel.raleigh@stonybrook.edu, Phone +1 631 632 4547.

[‡]These authors contributed equally to the work

Supporting Information. Supporting information is available free of charge at: http://pubs.acs.org. A table showing the fraction of vesicles that bind peptide for hIAPP and disulfide free variants, a figure showing ^{19}F NMR spectra of HFIP standards and a peptide sample reconstituted after lyophilization for 12 hr, a figure showing FRET measurements of hIAPP and variants binding to LUVs, a figure showing amyloid formation of hIAPP and variants in 20mM Tris buffer pH 7.4, and a figure showing the predicted helical content of hIAPP and variants as determined by AGADIR (PDF).

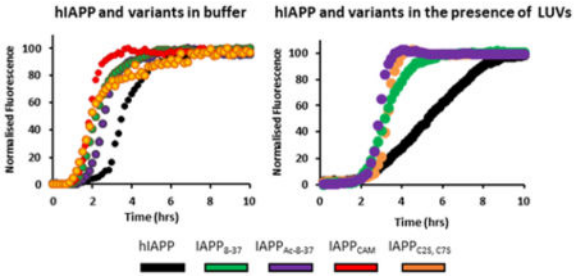

Keywords

Amylin; Amyloid; Disulfide; Islet Amyloid Polypeptide; Peptide Membrane Interactions

INTRODUCTION

Amyloid formation plays a critical role in the pathology of over 25 human diseases, including neurodegenerative diseases such as Alzheimer's, Huntington's and Parkinson's disease, as well as the metabolic disease type II diabetes (T2D). Islet amyloid polypeptide (hIAPP, also known as amylin,) is a 37-residue neuropancreatic hormone which plays a role in glucose homeostasis, and is co-secreted with insulin from the β-cells. IAPP helps to regulate satiety and gastric emptying by binding to receptors in the brain, and acts locally to suppress glucagon release from α-cells[1, 2]. Islet amyloid is a pathological hallmark of T2D and formation of islet amyloid deposits in the islets of Langerhans contributes to a reduction in β-cell mass in T2D and to islet transplant failure[3–6]. The mechanisms of amyloid formation by IAPP *in vitro* and *in vivo* are not well understood and the sequence determinates of IAPP amyloidogenicity have yet to be fully elucidated. Here we focus on the role of the conserved disulfide bridged loop on IAPP induced toxicity and on amyloid formation in solution and in the presence of model membranes composed of large unilamellar vesicles (LUVs).

Among proteins associated with amyloidosis, over half contain disulfide bonds[7]. In other systems, removal of disulfide bonds has been documented to lead to changes in aggregation rates, fibril morphology, and toxicity[8, 9]. Human IAPP (hIAPP) contains an amidated C-terminus as well as a disulfide loop formed between Cys-2 and Cys-7 that is strictly conserved (Figure 1). All organisms studied to date possess this disulfide bond, including variants that do not form amyloid, and very few mutations are found within the first 8 residues of IAPP[10, 11]. The disulfide bond is hypothesized to play a key role in receptor binding[12]. However, the contribution of the loop to amyloid formation is not well understood. The molecular mechanism of IAPP aggregation to produce amyloid is still unknown, but multiple key steps have been proposed. IAPP aggregation in solution has been conjectured to proceed via a helical intermediate and there is good evidence that IAPP transiently populates helical structure during model membrane mediated aggregation[13–17] β-hairpin dimers have been proposed to play a role in the initial steps of IAPP aggregation, while recent experiments have shown that the development of β-sheet structure during the aggregation of IAPP *in vitro* may involve formation of a transient non-native β-sheet[1819, 20]

The one thing all of these models have in common is that they ascribe no direct role to the disulfide bridged loop.

The structural restrictions imposed by the disulfide bond on the 1–7 segment led to the early hypothesis that it does not contribute to the process of amyloid formation, since the structural constraints imposed by the disulfide are not compatible with the cross-β structure of the core of the mature fibril. All current models of hIAPP amyloid fibrils place the loop resides outside of the fibril core[21–23]. This has led to the use of a truncated version of hIAPP composed of residues 8–37 as a surrogate for full length hIAPP in some biophysical experiments, presumably because the truncated polypeptide is easier to prepare. However, the presence of the loop could still impact the kinetics of amyloid formation. The loop might play a protective role and slow amyloid formation by either inhibiting oligomerization that leads to amyloid formation, or by stabilizing oligomers that are off-path from amyloid formation[24, 25]. Conversely the disulfide might enhance amyloid formation by promoting on pathway oligomerization or by inhibiting off pathway oligomerization. Along these lines, studies with an N-terminal fragment of hIAPP composed of residues 1–8 have shown differences in the propensity of the oxidized and reduced fragments to oligomerize, with the disulfide-less variant having a higher tendency to aggregate[26]. An intact disulfide did not completely inhibit aggregation of this fragment, but it did reduce its tendency to self-associate. Removal of the disulfide in the fragment has been proposed to lead to an increase in intermolecular hydrogen bonding which promotes oligomerization; i.e. the disulfide plays a protective role by reducing intermolecular contacts.

Removal of the disulfide might also alter the conformational propensities of unaggregated hIAPP. NMR experiments have revealed that hIAPP and the non-amyloidogenic variant rat IAPP have a propensity to transiently sample helical ϕ,ψ angles between residues 5 and 22 [13, 27]. Computational studies suggest that the removal of the disulfide impacts the structure of hIAPP in the lag phase by diminishing the helical content of the polypeptide[24, 2829] and recent NMR studies of hIAPP at pH 5.3 in various concentrations of oxidized and reduced gluthaione have shown that reduction of the disulfide leads to a reduction in helical propensity over residues 7 to 17.[30] The presence or absence of the disulfide bridged loop might also contribute to aggregation by altering the mechanical stability of the amyloid fibers. A change in fiber stability can alter the breakage rate of fibers; increased breakage leads to a more rapid production of fibers ends which in turn promotes amyloid formation via secondary nucleation[31].

In this work, we investigate the role of the disulfide loop in the context of *in vitro* aggregation and toxicity to cultured INS-1 β-cells. We also examine the role of the disulfide bond in membrane catalyzed amyloid formation and assess the effect of the disulfide on the ability of hIAPP to induce membrane leakage, using large unilamellar vesicles (LUVs). IAPP membrane interactions can accelerate amyloid formation and IAPP membrane interactions have been proposed to play a role in IAPP toxicity[14, 15, 32–34]. We find that removal of the disulfide has no detectable effect on hIAPP toxicity *in vitro,* but accelerates amyloid formation in homogenous solution and in the presence of LUVs. Removal of the disulfide also reduces hIAPP induced leakage for LUVS composed of 1-palmitoyl-2-oleoyl-

sn-glycero-3-phosphocholine (POPC) and 1-palmitoyl-2-oleoyl-*sn*-glycero-3-phospho-L-serine (POPS) and has smaller effects on LUVs which contain cholesterol.

MATERIALS AND METHODS

Synthesis and purification of IAPP

Peptides were synthesized using a CEM Liberty microwave peptide synthesizer, on a 0.10 mmol scale with 9-fluorenylmethoxycarbonyl (Fmoc) chemistry. 5-(4′-Fmoc-aminomethyl-3′,5-dimethoxyphenol) valeric acid (PAL-PEG) was used to afford an amidated C-terminus. Pseudoproline dipeptide (oxazolidine) dipeptide derivatives were used as previously described to improve the yield[35, 36]. All β-branched residues, pseudoproline dipeptides, and the first amino acid attached to the resin were double coupled. For $IAPP_{Ac8–37}$, capping of the N-terminus was achieved by treating the peptide after final deprotection with a solution of acetic anhydride, diisopropylethylamine, and DMF in a 5 : 2 : 93 ratio (v/v%). The peptide was microwaved in the capping solution for two minutes. Peptides were cleaved using trifluoroacetic acid (TFA) with triisopropylsilane (TIPS), and H_2O as scavengers. Cleaved peptides were subsequently dissolved in 15% acetic acid (v/v) and lypophilized prior to formation of the disulfide and purification. The internal disulfide bond in wild type hIAPP was formed by dissolving dry peptide into 100% DMSO at a concentration of 15mg/mL and incubating at room temperature for three days. $IAPP_{CAM}$ was synthesized as previously described[37]. Briefly, pure hIAPP was incubated in a solution of 13mM DTT, 6M GdnHCl, 0.19M Tris HCl, and 10% DMSO at pH 8.0 for 4 hours at 4°C under nitrogen gas to reduce the peptide. After reduction, iodoacetamide was added to the cocktail to a final concentration of 8mM, and the reaction allowed to proceed for four hours at 4°C in the dark. The reaction was quenched with 80mM 2-mercaptoethanol. Peptides were purified via reverse-phase high performance liquid chromatography (RP-HPLC) using a Higgins Analytical Proto 300 C18 Preparative column. Residual scavengers were removed using an HFIP extraction procedure. Purified peptide was dissolved in neat HFIP to a concentration of 10mg/mL, the solution was incubated for four hours, filtered with a 0.45μM GHP membrane filter, and purified via HPLC. If necessary, the process was repeated. Masses of purified peptides were measured using matrix-assisted laser desorption time-of-flight mass spectrometry (MALDI-TOF). hIAPP expected 3903.6, observed 3902.9; $IAPP_{8-37}$ expected 3183.4, observed 3148.0; $IAPP_{Ac8-37}$ expected 3225.5, observed 3226.1, $IAPP_{C2S, C7S}$, expected 3872.2, observed 3874.1; $IAPP_{CAM}$ expected 4019.6, observed 4019.0.

Transmission Electron Microscopy

Transmission Electron Microscopy (TEM) images were taken at the Central Microscopy Imaging Center at Stony Brook University. At the conclusion of a thioflavin-T monitored kinetic experiment, 15μL aliquots were taken from sample wells and blotted onto a 300-mesh copper grid for one minute, followed by negative staining with uranyl acetate for one minute.

Peptide stock and sample preparation

Stock solutions were prepared by dissolving lyophilized peptide into 100% hexafluoroisopropanol (HFIP) to a target concentration of 1.6mM. Concentration was determined by lyophilizing a 10 μL aliquot of HFIP stock for at least 12 hours. Dry peptide was then dissolved in 100 μL 20mM Tris buffer, pH 7.4, and absorbance measured at 280nm, using an extinction coefficient of 1620 $M^{-1}cm^{-1}$ for hIAPP and 1490 $M^{-1}cm^{-1}$ for variants lacking cysteines. Aliquots for experiments were then lyophilized for at least 12 hours prior to reconstitution. The amount of residual HFIP in the final samples was less than $4.6x10^{-5}$ mole % as judged by ^{19}F- NMR (Figure S1). Calibration samples for NMR experiments were prepared in 90%DMSO/10% DMSO-d6 with various concentrations of HFIP (1 mM, 100 μM, 50 μM). Peptide stock was lyophilized for 12hr and reconstituted in 90%DMSO/10%DMSO-d6. ^{19}F- NMR experiments were conducted on a Bruker 400 MHz Nanobay Spectrometer at 25°C, and collected with 16 scans with a sweep width of 237.35 ppm

Fluorescence Assays

Aliquots of HFIP stock solution were lyophilized overnight and reconstituted in phosphate buffered saline (PBS,10mM Sodium Phosphate, 140mM KCl) or 20mM Tris at pH 7.4 for kinetic assays. Final peptide concentration was 16 μM, with thioflavin-T added from a stock solution to a final concentration of 32 μM. Black Corning 96-well non-binding plates were used for ThT assays. Plates were sealed with polyethylene sealing tape and a clear lid was used. Wells at the edge of the plate were not used. Unused wells were filled with buffer. Fluorescence measurements were taken on a Beckmann Coulter DTX 880 plate reader, with a multimode detector using an excitation wavelength of 430nm and an emission wavelength of 485nm. Readings were taken from the bottom of the wells in ten minute intervals with no additional shaking. For experiments with lipid vesicles, a quartz plate was used, as plates coated with a non-binding surface led to LUV leakage. Experiments conducted in the presence of membranes were initiated by adding 400 μM LUVs. Three parallel samples using different solutions of hIAPP were tested for each experiment. All fluorescence assays were performed at 25 °C.

Cytotoxicity Assays

Rat INS-1 β-cells were seeded into 96-well plates at a density of 35,000–40,000 cells per well, 15–24 hours prior to the start of an experiment. Peptides were dissolved into complete RPMI and incubated with the cells for 24 hours prior to measuring cell viability, which was determined by Alamar Blue reduction assays. Alamar Blue stock solution was diluted tenfold in RPMI medium and incubated with the cells for five hours at 37 °C. Fluorescence was measured using a Beckman Coulter DX880 plate reader, using an excitation wavelength of 530 nm and reading the emission at 590 nm. Cell viability measurements were normalized with respect to untreated control cells.

Preparation of Large Unilamellar Vesicles

POPC, POPS, and cholesterol were obtained from Avanti Polar Lipids. The lipid concentrations were determined by dry weight. Multilamellar vesicles (MLV) were prepared

by dissolving lipids in chloroform in a glass tube at the desired concentration. Mixtures were evaporated with nitrogen gas and were dried in vacuum for one hour to completely remove the residual organic solvent. The dry lipids were then dispersed in Tris buffer (20 mM Tris·HCl, 100 mM NaCl at pH 7.4) and agitated at 55 °C for at least 20 minutes. Samples were cooled to room temperature before use. Large unilamellar vesicles (LUVs) were prepared from MLVs by subjecting the MLVs to 10 freeze-thaw cycles and then passing through a 100 nm polycarbonate filter (Avanti Polar Lipids) 21 times to obtain vesicles of uniform size. The phospholipid concentration was determined by the method of Stewart [38]. For the membrane leakage experiments, LUVs encapsulated with carboxyfluorescein were prepared using the same protocol except that carboxyfluorescein was dissolved in Tris buffer (20 mM Tris·HCl, 100 mM NaCl at pH 7.4) at a concentration of 80 mM before hydration. Nonencapsulated carboxyfluorescein was removed from LUVs using a PD-10 desalting column (GE Healthcare Life Sciences) with elution using 20 mM Tris·HCl, 100 mM NaCl buffer, pH 7.4. Dynamic light scattering was used to check the effective diameter and polydispersity of each vesicle before use. A fresh vesicle solution was used for each experiment.

Dynamic Light Scattering

Dynamic light scattering experiments were performed on a NanoBrook 90Plus Particle Size Analyzer (Brookhaven Instruments) with a 35 mW red diode laser. The wavelength of irradiation was 640 nm. Membrane samples were prepared to a final concentration of 40 μM with 20 mM Tris·HCl, 100 mM NaCl buffer (pH 7.4). For each sample, three runs were taken at 25 °C with one minute per run. The average diameter (effective diameter) and the distribution width (polydispersity) were calculated using the 90Plus Particle Sizing Software.

Membrane Permeability Assays

Leakage experiments were performed using a Beckman Coulter DTX880 plate reader. The excitation and emission wavelength filters were 485 nm and 535 nm, respectively. Samples were incubated in a 96-well quartz microplate at 25 °C. Peptide concentration was 20 μM and the concentration for LUVs encapsulated with dye was 400 μM. The fluorescence signal of the carboxyfluorescein-encapsulated LUVs was continuously measured during the course of each experiment. The maximum leakage for totally disrupted vesicles was induced by adding the detergent Triton X-100 to a final concentration of 0.2 % (vol/vol).

The percent change in carboxyfluorescein fluorescence is calculated as:

$$\text{Percent Fluorescence Change} = 100 \times [F(T) - F_{baseline}]/(F_{max} - F_{baseline}) \quad (1)$$

Where F(T) is the fluorescence intensity at time T, F_{max} is the fluorescence intensity when all of the vesicles have been disrupted and $F_{baseline}$ is the base line fluorescence observed before addition of hIAPP. F_{max} was experimentally determined by disrupting the vesicles with Triton X-100. All of the leakage experiments were repeated three times using different IAPP stock solutions.

Sucrose Density Gradient Centrifugation Assays

Sucrose gradient centrifugation studies were performed using a Beckman L8–55M ultracentrifuge with an SW-60 rotor. Sucrose gradients were prepared by freezing 3.5 ml of 10% (w/w) sucrose solution in centrifuge tubes at –20 °C overnight and thawing to room temperature. Sucrose concentrations in the fractions were estimated with a refractometer and the highest density was 20% sucrose (bottom layer) and the lowest 5 % sucrose (top layer). Vesicles were labeled with 2 mole percent NBD-DOPE for visualization. Vesicles were incubated with hIAPP, $IAPP_{C2S, C7S}$ and truncated $IAPP_{8-37}$, respectively, until amyloid formation was complete. 500 μL aliquots of this solutions were then loaded on top of the gradient and centrifuged at 37,500 rpm (19,000 g) for 45 minutes. Vesicles that bind substantial peptide migrate to the bottom of the gradient while those that do not float on top. The two lipid-containing layers were removed separately and then diluted to 1.0 ml with Tris buffer. The amount of NBD-DOPE in each layer was quantified using a SPEX FluoroLog 3 spectrofluorometer with excitation and emission wavelengths at 465 nm and 534 nm. Background intensities in samples lacking fluorescent probe were subtracted. All of the sucrose gradient experiments were repeated three times using different IAPP stock solutions. The presence or absence of peptide in each layer was quantified by measuring Tyr absorbance at 280nm, using a Beckman-Coulter DU730 UV/Vis spectrophotometer. The 1.0ml diluted samples (described above) were vortexed before recording absorbance spectra.

Results

Design of hIAPP variants to study the role of the Cys-2 Cys-7 disulfide bond

A series of peptides were synthesized that eliminated the disulfide bond through various modifications (Figure 1). A pair of truncated IAPP variants were prepared that lack the first seven residues, $IAPP_{8-37}$ and an N-terminal acetylated variant of this molecule $IAPP_{Ac8-37}$. Removal of the free N-terminus by acetylation reduces the net charge of the peptide, and introduces an additional hydrogen bond acceptor. These modifications are expected to enhance any tendency the truncated analog may have to sample helical structure in the monomeric state relative to the unacetylated variant, since they remove unfavorable charge helix dipole interactions and provide a potential helix N-capping group. Two full length variants were prepared; one caps the cysteines using carbamidomethylation ($IAPP_{CAM}$). The CAM group prevents reformation of the disulfide, but adds addition hydrogen bonding functionality to the sidechain and is bulkier than a Cys. Consequently, we also made a more conservative replacement. Traditionally Cys to Ala replacements are used to eliminate disulfide bonds found in the hydrophobic environment of globular proteins, but Ala is not a conservative replacement for a solvent exposed disulfide and Ser is often used for solvent exposed Cys residues. Ser is closer to Cys in polarity than Ala and is a much better approximation to an iso-steric replacement. In addition, the higher helical propensity of Ala, could perturb the secondary structure of IAPP in the unaggregated state, especially as residues 5 through 22 transiently sample helical φ,ψ angles in the unaggregated state[13]. Consequently, both cysteine residues were replaced with serine ($IAPP_{C2S, C7S}$).

This set of polypeptides provides a diverse set of disulfide-free variants, allowing a rigorous test of the effects of removing the disulfide bond from IAPP. These variants were also

chosen to allow comparison to previous studies that used truncated variants of hIAPP to study the aggregation kinetics of disulfide-free IAPP variants in mixed-organic solvents [37].

The disulfide bond is not required for cytotoxicity

We first examined the role of the conserved disulfide in hIAPP induced cytotoxicity using the $IAPP_{C2S, C7S}$ double mutant since it represents the most conservative modification. Cell viability was monitored by Alamar Blue reduction assays using INS-1 β-cells (Figure 2). Wild type hIAPP and $IAPP_{C2S, C7S}$ were examined at 20, 30 and 40 μM. These concentrations are typical of those used in cell viability assays of the effect of IAPP variants. Both hIAPP and $IAPP_{C2S, C7S}$ reduce cell viability and there is no statistically significantly difference between the effects of the two polypeptides. Treatment with 20 μM peptide reduced cell viability relative to untreated cells to 60 to 70% cell viability, i.e. a 30–40% reduction. 30 μM peptide lead to a further decrease in cell viability to between 40 and 30% while treatment with 40 μM of either peptide reduced cell viability to 20% relative to untreated control.

Disulfide-less variants form amyloid more rapidly than hIAPP

The time course of amyloid formation was monitored using fluorescence detected thioflavin-T binding assays and the presence of amyloid confirmed using transmission electron microscopy (TEM). Thioflavin-T assays provide kinetic information and are straightforward to conduct, but thioflavin-T is an extrinsic dye and can both yield false positives and false negatives. False negatives have been documented with IAPP variants[39] Thus, TEM was used to verify the formation of amyloid. Thioflavin-T based assays have been shown to accurately monitor the kinetics of hIAPP amyloid formation under the conditions of these experiments[40]. The relationship between the final thioflavin-T fluorescence intensity and the amount of amyloid fibers formed is not clear, thus we do not quantitatively interpret the final thioflavin-T fluorescence intensity. Each variant exhibits behavior typical of an amyloidogenic protein, with a lag phase followed by a growth phase which leads to a final plateau phase.

Removal of the disulfide loop leads to faster amyloid formation as judged by T_{50}, the time a given sample takes to reach half the maximum fluorescent intensity in a thioflavin-T assay (Figures 3A, 3B). Variants without a disulfide all form amyloid roughly 1.5 to 1.8 times faster than wildtype hIAPP in phosphate buffer saline (PBS, 10mM phosphate, 140 mM KCl, pH 7.4). The T50 values for the two truncated variants are 1.9± 0.3 hours for $IAPP_{8-37}$ and 2.3 ± 0.1 hours for $IAPP_{Ac8-37}$ under the conditions of these assays, compared to 3.4 ± 0.3 hours for hIAPP. The full length disulfide-free variants also exhibited more rapid amyloid formation than wild type hIAPP as judged by the reduced T_{50}, with $IAPP_{CAM}$ showing a T_{50} of 1.9±.03 hours and $IAPP_{C2S, C7S}$ a T_{50} of 1.9±0.1 hours. TEM studies confirm that all variants form amyloid formation, showing dense mats of fibrils (Figure 3C).

The experiments described above were conducted using PBS. We also studied the effect of removing the disulfide by conducting experiments in Tris buffer, since Tris is also widely used in studies of IAPP amyloid formation and hIAPP amyloid formation is slower in Tris compared to PBS[41]. The disulfide-less variants also aggregate faster than hIAPP in 20mM

Tris buffer, (Figure S3A). Under these conditions, the T_{50} for wildtype hIAPP is 8.9±0.7 hours while the T_{50} values of $IAPP_{8-37}$ and $IAPP_{Ac8-37}$ are 1.8 ± 0.6 hours and 1.45 ± 0.4 hours respectively, representing a 5 to 6 fold reduction in T_{50} respectively. $IAPP_{CAM}$ has a T_{50} of 4.2±0.1 hours, and $IAPP_{C2S\ C7S}$ 4.1±0.1 hour (Figure S3B) under these conditions. The reason for the greater relative enhancement in Tris for the truncated variants compared to the enhancement observed in PBS is not clear, although it is known that phosphate in general accelerates hIAPP amyloid formation relative to Tris and that the identity of the anion has a strong effect on IAPP aggregation. Perhaps the general enhancement in aggregation due to phosphate makes it more difficult to detect differences due to the loss of the disulfide[41]. TEM studies again confirm that these variants form amyloid, showing dense mats of fibrils (Figure S3C).

Disulfide- less variants also aggregate more quickly than wild type in the presence of LUVs

We also monitored amyloid formation in the presence of LUVs prepared with mixed lipid compositions. One set of experiments was conducted using LUV's containing 75 mol% POPC and 25 mol% POPS and a second using LUV's containing 50 mol% POPC, 10 mol% POPS, and 40 mol% cholesterol. The first was chosen to mimic conditions used for biophysical studies of membrane-hIAPP interactions that have been reported in the literature, and the second because cholesterol has been shown to modulate hIAPP membrane interactions[42, 43]. A 1:20 peptide to lipid ratio was used for both systems to ensure compatibility with prior biophysical studies[43–45]. All of the peptides, including wild type hIAPP, aggregate faster in the presence of LUVs composed of 75 mol% POPC and 25 mol% POPS relative to the time required in the absence of LUVs and removal of the disulfide further accelerates amyloid formation. The disulfide less variants aggregate in roughly 60% of the time that hIAPP does under these conditions (Figure 4A). hIAPP has a T_{50} value of 5.3±0.6 hours., whereas the truncated variants $IAPP_{8-37\ and}$ $IAPP_{Ac8-37}$ have T_{50} values of 3.2 ±0.3 and 2.9±0.3 respectively. Full length $IAPP_{C2S,\ C7S}$ has a T_{50} value of 3±0.4 hours. The presence of a high concentration of anionic lipid in the model membrane likely facilitates binding of IAPP to the membrane, as all of the peptides have a net positive charge at pH 7.4, however the aggregation profiles of all variants that lack the disulfide are broadly similar, despite the differences in their predicted net charge and there is little difference in the value of T_{50} for the truncated variants and the full length $IAPP_{C2S,\ C7S}$. This indicates that factors aside from net charge contribute to membrane mediated amyloid formation since the net charge of the variants ranges from +4 to +3 ($IAPP_{C2S,\ C7S}$) to +2 to +1 ($IAPP_{Ac8-37}$) at pH 7.4 depending upon the pk_a of the His residue and the N-terminus. Amyloid formation was confirmed at the conclusion of the thioflavin-T monitored experiments via TEM imaging (Figure 4B). Each sample contained amyloid fibrils.

The same trend is observed with vesicles containing 50 mol% POPC, 10 mol% POPS, and 40 mol% cholesterol (Figure 5), however the overall time scale of aggregation is lengthened compared to vesicles composed of 75 mol% POPC / 25 mol% POPS. This is expected given the reduction in anionic lipid concentration, and the presence of cholesterol; both of which are known to slow LUV induced amyloid formation[44, 46]. The T_{50} for hIAPP under these conditions is 20.9±1.7 hours, while the values for $IAPP_{8-37}$ and $IAPP_{Ac8-37}$ are 8.7±1.0 and

7.6±.8 hours respectively. $IAPP_{C2S, C7S}$ has a T_{50} of 11.33±1.4 hours. Thus, elimination of the disulfide leads to a 2 to 3 fold decrease in T_{50} under these conditions irrespective of the method of removal.

IAPP induced membrane leakage is reduced for variants which lack the disulfide

hIAPP induced leakage of LUVs was studied using carboxyfluorescein based assays. LUVs were loaded with carboxyfluorescein. The dye fluorescence is self-quenched, owing to the high dye concentration in the interior of the LUV. Leakage allows the dye to diffuse into solution, relieving self-quenching and leading to an enhancement in observable fluorescence. hIAPP induces the most leakage of the peptides studied for both LUV preparations. After 10 minutes of incubation hIAPP induces 35% leakage of the 75 mol% POPC, 25 mol% POPS LUVs. 58% leakage is observed after incubation for a time sufficient for amyloid formation to reach completion (Figure 6A). Variants without the disulfide bond lead to less membrane leakage at both short and long times. All variants reached their maximum leakage after two hours. The two truncated variants lead to the smallest amount of membrane leakage, 2% after 10 minutes incubation for both $IAPP_{8-37}$ and $IAPP_{Ac8-37}$. The observed leakage increased to 31 and 35% after 2 hours incubation for the unacetylated and acetylated variants respectively. Incubation with the $IAPP_{C2S, C7S}$ lead to higher leakage than the truncated variants: 12% after 10 minutes and 43% after 2 hours, but the level of leakage was still lower than induced by wild type hIAPP (Figure 6A, 6B). The decreased leakage observed for the C2S, C7S mutant relative to wild type is interesting given that we detected no significant difference in the cytotoxicity of the two polypeptides. Membrane disruption has been proposed to contribute to IAPP toxicity in vivo, but the lack of a correlation between toxicity and membrane permeability of the mixed POPC, POPS LUVs observed here indicates that there is not a one-to-one correspondence between experiments conducted with simple standard model membranes and the toxic effects of IAPP. This result is consistent with earlier studies that examined a different set of IAPP variants[45].

In the presence of vesicles composed of 40 mol% cholesterol, 10 mol% POPS and 50 mol% POPC, leakage takes considerably longer to reach a plateau (Figure 7A). There is also a noticeable decrease in initial leakage, as well as in the final change in fluorescence after plateauing relative to vesicles without cholesterol (Figure 7B). After ten minutes of incubation, all variants lead to less than a 2% change in fluorescence. By the conclusion of the experiments, incubation with hIAPP results in a final fluorescence change of 30% and the $IAPP_{C2S, C7S}$ variant caused a 28% change in fluorescence. Both truncated variants showed a smaller change in fluorescence during leakage assays than did the full length sequences, with $IAPP_{8-37}$ inducing 17% change in fluorescence and $IAPP_{Ac8-37}$ a 19% change. Overall, the data reveals that the disulfide bridged loop plays a role in membrane leakage.

We have previously observed a strong positive correlation between the extent of leakage after long time incubation and the fraction of vesicles that bind wild type human IAPP. We performed peptide binding assays using sucrose gradient experiments to determine if this correlation can help to rationalize the differences observed in induced leakage by hIAPP and the disulfide less variants. We first used a FRET based assay to confirm that peptide binding

to the LUVs is saturated under the conditions of our experiments (Supporting Figure S2). Sucrose gradient measurements were then performed to deduce the fraction of vesicles that bound significant amounts of peptide. LUVs were labeled with 2 mol% of the fluorescence lipid probe NBD-DOPE and were incubated with hIAPP, $IAPP_{C2S, C7S,}$ $IAPP_{8-37}$, respectively, for a time long enough to form amyloid. The LUV-peptide mixtures were then centrifuged in a 5 to 20 percent sucrose gradient. Two fractions were observed in the presence of peptides; a denser fraction containing vesicles with bound peptide migrates to the bottom, and a lighter fraction containing vesicles with little peptide bound floats at the top of the gradient, which is the same position observed for control LUVs in the absence of peptide. The fact that there were two clear fractions indicated that not all vesicles bound significant amounts of peptide under the conditions examined. We used Tyr absorbance to confirm that the non-pelleting (lighter) layer did not contain peptide while the denser fraction did. There is a correlation between the fraction of vesicles which bound significant amounts of peptide and the percent leakage after incubation for these peptides. The larger percentage of vesicles that bound hIAPP compared to the variants that lack the disulfide bond correlates with the increased level of leakage caused by the wild type hIAPP. For the vesicles made up of 75 mol% POPC and 25 mol% POPC, 63% of the LUVs bound a significant amount of wild type hIAPP and pelleted, while 51% of the vesicles bound significant amounts of the $IAPP_{C2S\ C7S}$ double mutant and 46% bound truncated $IAPP_{8-37}$ variant (Table S1). Thus, the lower levels of leakage observed for $IAPP_{C2S\ C7S}$ and the truncated $IAPP_{8-37}$ variant in 25 mol% POPS and 75 mol% POPC vesicles correlate with a reduction in the fraction of vesicles that bind peptide (Table S1). This is also true for the 10 mol% POPS, 40 mol% cholesterol and 50 mol% POPC vesicles (Table S1).

Discussion

The data presented here indicates that the disulfide bond plays a protective role and slows amyloid formation by hIAPP in acqueous buffer. Although the loop does not prohibit self-association, aggregation proceeds at an accelerated rate in its absence under all conditions studied. The results reported here are in agreement with solution studies of oxidized and reduced wild type hIAPP at pH 5.3, but differs slightly from earlier studies of IAPP amyloid formation in mixed H_2O hexafluroisopropanol (HFIP)[37]. That work showed that the disulfide affected secondary nucleation, but its removal had a smaller impact on the T_{50} for amyloid formation than observed here in buffer. The rate of IAPP amyloid formation is known to be considerably enhanced by even low levels of HFIP[47], and it is not known if the mechanism of amyloid formation is the same in the presence of HFIP, thus it is difficult to compare studies performed with HFIP as a co-solvent to those performed in buffer, even when the volume fraction of HFIP is low. The properties of mixed HFIP water systems are complex and HFIP forms clusters in aqueous solutions at mole fractions higher than used in studies of hIAPP amyloid formation[48]. Cluster formation has not been investigated at lower HFIP concentrations, but it is possible that they form, and may contribute to the acceleration of IAPP amyloid formation.

Faster amyloid formation relative to wild type is observed for variants that lack the disulfide in the presence of the two LUVs tested. The C2S, C7S double mutant does not induce the same level of model membrane leakage as wild type in the cholesterol free system,

reinforcing the view that permeabilization of simplified model membranes does not directly correlate with IAPP toxicity. The reduced leakage observed for the variants that lack the disulfide bond correlates with a reduced fraction of vesicles that bind significant amounts of polypeptide.

The disulfide bond is expected to promote the tendency to sample helical structure in the 8–22 region[30] and the effect of removing the disulfide upon amyloid formation might be due to modulation of helical propensity especially as the 8–18 region is thought to be important for initial contacts during IAPP self-assembly to form amyloid in solution and for IAPP IAPP interactions on model membrane surfaces [49, 50]. Alternatively, the disulfide bridged segment might make contacts that slow amyloid formation or could prevent the formation of other contacts that are favorable for amyloid formation. Removal of the disulfide might also alter the mechanically stability of IAPP amyloid fibers and alter the breakage rate. Studies of the two truncated variants argue that the effect of removal of the disulfide is not entirely due to changes in helix propensity as the truncated variants, $IAPP_{8\text{-}37}$ and $IAPP_{Ac8\text{-}37}$, have little difference in their propensity to form amyloid, as defined by T_{50} values, but do have clear differences in helix propensity as predicted by the AGADIR algorithm[51] (Supporting Figure-S4), with the algorithm predicting that $IAPP_{Ac8\text{-}37}$ has a higher helical propensity than $IAPP_{8\text{-}37}$ across the 8–15 region (Supporting Figure S4B). $IAPP_{C2S,\ C7S}$ is predicted to have nearly identical helical content in the 8–15 region as $IAPP_{Ac8\text{-}37}$. These observations suggest that the truncated variants and the $IAPP_{C2S,\ C7S}$ mutant form amyloid faster than wild type hIAPP because of loss of the disulfide and modulation of inter peptide contacts and/or effects on secondary nucleation rather than just because of significant changes in helical propensity.

Helical intermediates have been proposed to play a role in amyloid formation by hIAPP, but their exact significance has yet to be fully defined and studies with variants of IAPP that contain a pair of helix breaking D-Pro replacements at positions 15 and 16 have shown that they do not affect the rate of amyloid formation in solution, a result which is broadly consistent with the results reported here in the sense that modulating the helix propensity of the 8-37 variants did not significantly alter the value of T_{50}[13, 16, 17, 52, 53].The data reported here is also consistent with studies of short N-terminal fragments of IAPP that have shown that lack of the disulfide leads to more rapid aggregation and alters intermolecular interactions in this small peptide.[54] That work and the current study are consistent with the disulfide exerting its effect on amyloid formation by, in part, mediating peptide-peptide interactions rather than solely by its effect on the helical propensity of the monomer.

In the presence of lipid vesicles, aggregation proceeds via a membrane mediated process in which hIAPP associates on the membrane, possibly via formation of helical structure and then undergoes further oligomerization before forming amyloid[14, 55]. Membrane mediated IAPP amyloid formation is believed to occur on the surface of the vesicle and a simple rationalization of the data reported here is that the disulfide modulates IAPP-IAPP interactions on the membrane surface as well as in homogenous solution.

The membrane leakage data indicates that the N-terminal seven residues play a role in modulating the ability of IAPP to permeate model lipid vesicles. $IAPP_{8\text{-}37}$ and $IAPP_{Ac8\text{-}37}$

showed a significantly reduced capacity to induce leakage in vesicles with and without cholesterol. $IAPP_{C2S, C7S}$ was able to induce more leakage than the truncated variants, but less than hIAPP in the cholesterol free vesicles. The difference in leakage between hIAPP and the disulfide less variants is diminished in vesicles with 40 mole percent cholesterol. The data presented here reveals a strong correlation between the fraction of vesicles that bind peptide and induce leakage, indicating that the disulfide contribution to binding also affects leakage.

Supplementary Material

Refer to Web version on PubMed Central for supplementary material.

Acknowledgments

We thank Prof Steve Bourgault for helpful discussions. We thank Ms. Natalie Stenzoski and Dr. Fang Liu for help with ^{19}F-NMR measurements. This work was supported by US National Institutes of Health grants GM078114 to DPR and a grant from the American Heart Association, 17SDG33410350 to AA as well as by funds from the Diabetes Research Program at NYU Langone Medical Center to AMS. ZR was supported in part by a GAANN fellowship from the US Department of Education.

References

1. Westermark P, Andersson A, Westermark GT. Islet Amyloid Polypeptide, Islet Amyloid, and Diabetes Mellitus. Physiol Rev. 2011; 91:795–826. [PubMed: 21742788]
2. Akter R, Cao P, Noor H, Ridgway Z, Tu L-H, Wang H, Wong AG, Zhang X, Abedini A, Schmidt AM, Raleigh DP. Islet Amyloid Polypeptide: Structure, Function, and Pathophysiology. Journal of Diabetes Research. 2016; 2016:18.
3. Westermark P, Wernstedt C, Wilander E, Hayden DW, O'Brien TD, Johnson KH. Amyloid fibrils in human insulinoma and islets of Langerhans of the diabetic cat are derived from a neuropeptide-like protein also present in normal islet cells. Proceedings of the National Academy of Sciences. 1987; 84:3881–3885.
4. Cooper GJ, Leighton B, Dimitriadis GD, Parry-Billings M, Kowalchuk JM, Howland K, Rothbard JB, Willis AC, Reid KB. Amylin found in amyloid deposits in human type 2 diabetes mellitus may be a hormone that regulates glycogen metabolism in skeletal muscle. Proceedings of the National Academy of Sciences. 1988; 85:7763–7766.
5. Udayasankar J, Kodama K, Hull RL, Zraika S, Aston-Mourney K, Subramanian SL, Tong J, Faulenbach MV, Vidal J, Kahn SE. Amyloid formation results in recurrence of hyperglycaemia following transplantation of human IAPP transgenic mouse islets. Diabetologia. 2009; 52:145–153. [PubMed: 19002432]
6. Potter KJ, Abedini A, Marek P, Klimek AM, Butterworth S, Driscoll M, Baker R, Nilsson MR, Warnock GL, Oberholzer J, Bertera S, Trucco M, Korbutt GS, Fraser PE, Raleigh DP, Verchere CB. Islet amyloid deposition limits the viability of human islet grafts but not porcine islet grafts. Proceedings of the National Academy of Sciences. 2010; 107:4305–4310.
7. Li Y, Yan J, Zhang X, Huang K. Disulfide Bonds in Amyloidogenesis Diseases Related Proteins. Proteins. 2013; 81:1862–1873. [PubMed: 23760807]
8. Mossuto MF, Bolognesi B, Guixer B, Dhulesia A, Agostini F, Kumita JR, Tartaglia GG, Dumoulin M, Dobson CM, Salvatella X. Disulfide Bonds Reduce the Toxicity of the Amyloid Fibrils Formed by an Extracellular Protein. Angewandte Chemie. 2011; 50:7048–7051. [PubMed: 21671315]
9. Sarkar N, Kumar M, Dubey VK. Effect of Sodium Tetrathionate on Amyloid Fibril: Insight into the Role of Disulfide Bond in Amyloid Progression. Biochimie. 2011; 93:962–968. [PubMed: 21354256]

10. Westermark P, Engström U, Johnson KH, Westermark GT, Betsholtz C. Islet amyloid polypeptide: pinpointing amino acid residues linked to amyloid fibril formation. Proceedings of the National Academy of Sciences of the United States of America. 1990; 87:5036–5040. [PubMed: 2195544]
11. Wu C, Shea JE. Structural Similarities and Differences Between Amyloidogenic and Non-Amyloidogenic Islet Amyloid Polypeptide (IAPP) Sequences and Implications for the Dual Physiological and Pathological Activities of These Peptides. PLoS Computational Biology. 2013; 9:e1003211. [PubMed: 24009497]
12. Barwell J, Gingell JJ, Watkins HA, Archbold JK, Poyner DR, Hay DL. Calcitonin and Calcitonin Receptor-Like Receptors: Common Themes with Family B GPCRs? British Journal of Pharmacology. 2012; 166:51–65. [PubMed: 21649645]
13. Williamson JA, Loria JP, Miranker AD. Helix Stabilization Precedes Aqueous and Bilayer-Catalyzed Fiber Formation in Islet Amyloid Polypeptide. Journal of Molecular Biology. 2009; 393:383–396. [PubMed: 19647750]
14. Jayasinghe SA, Langen R. Membrane interaction of islet amyloid polypeptide. Biochimica et Biophysica Acta (BBA) - Biomembranes. 2007; 1768:2002–2009. [PubMed: 17349968]
15. Hebda JA, Miranker AD. The Interplay of Catalysis and Toxicity by Amyloid Intermediates on Lipid Bilayers: Insights from Type II Diabetes. Annual Review of Biophysics. 2009; 38:125–152.
16. Wiltzius JJW, Sievers SA, Sawaya MR, Eisenberg D. Atomic structures of IAPP (amylin) fusions suggest a mechanism for fibrillation and the role of insulin in the process. Protein Sci. 2009; 18:1521–1530. [PubMed: 19475663]
17. De Carufel CA, Quittot N, Nguyen PT, Bourgault S. Delineating the Role of Helical Intermediates in Natively Unfolded Polypeptide Amyloid Assembly and Cytotoxicity. Angewandte Chemie International Edition. 2015; 54:14383–14387. [PubMed: 26440575]
18. Buchanan LE, Dunkelberger EB, Tran HQ, Cheng P-N, Chiu C-C, Cao P, Raleigh DP, de Pablo JJ, Nowick JS, Zanni MT. Mechanism of IAPP amyloid fibril formation involves an intermediate with a transient β-sheet. Proceedings of the National Academy of Sciences. 2013; 110:19285.
19. Dupuis NF, Wu C, Shea J-E, Bowers MT. The Amyloid Formation Mechanism in Human IAPP: Dimers Have β-Strand Monomer−Monomer Interfaces. Journal of the American Chemical Society. 2011; 133:7240–7243. [PubMed: 21517093]
20. Serrano AL, Lomont JP, Tu L-H, Raleigh DP, Zanni MT. A Free Energy Barrier Caused by the Refolding of an Oligomeric Intermediate Controls the Lag Time of Amyloid Formation by hIAPP. Journal of the American Chemical Society. 2017; 139:16748–16758. [PubMed: 29072444]
21. Kajava AV, Aebi U, Steven AC. The Parallel Superpleated Beta-Structure as a Model for Amyloid Fibrils of Human Amylin. Journal of Molecular Biology. 2005; 348:247–252. [PubMed: 15811365]
22. Luca S, Yau WM, Leapman R, Tycko R. Peptide Conformation and Supramolecular Organization in Amylin Fibrils: Constraints From Solid-State NMR. Biochemistry. 2007; 46:13505–13522. [PubMed: 17979302]
23. Wiltzius JJW, Sievers SA, Sawaya MR, Cascio D, Popov D, Riekel C, Eisenberg D. Atomic Structure of The Cross-Beta Spine of Islet Amyloid Polypeptide (Amylin). Protein Sci. 2008; 17:1467–1474. [PubMed: 18556473]
24. Wineman-Fisher V, Tudorachi L, Nissim E, Miller Y. The Removal of Disulfide Bonds in Amylin Oligomers Leads to the Conformational Change of the 'Native' Amylin Oligomers. Physical chemistry chemical physics : PCCP. 2016; 18:12438–12442. [PubMed: 27109452]
25. Laghaei R, Mousseau N, Wei G. Structure and Thermodynamics of Amylin Dimer Studied by Hamiltonian-Temperature Replica Exchange Molecular Dynamics Simulations. The Journal of Physical Chemistry B. 2011; 115:3146–3154. [PubMed: 21384830]
26. Ilitchev AI, Giammona MJ, Do TD, Wong AG, Buratto SK, Shea JE, Raleigh DP, Bowers MT. Human Islet Amyloid Polypeptide N-Terminus Fragment Self-Assembly: Effect of Conserved Disulfide Bond on Aggregation Propensity. Journal of the American Society for Mass Spectrometry. 2016; 27:1010–1018. [PubMed: 26894887]
27. Williamson JA, Miranker AD. Direct detection of transient α-helical states in islet amyloid polypeptide. Protein Sci. 2007; 16:110–117. [PubMed: 17123962]

28. Milardi D, Pappalardo M, Pannuzzo M, Grasso DM, La Rosa C. The role of the Cys2-Cys7 disulfide bridge in the early steps of Islet amyloid polypeptide aggregation: A molecular dynamics study. Chemical Physics Letters. 2008; 463:396–399.
29. Laghaei R, Mousseau N, Wei GH. Effect of the Disulfide Bond on the Monomeric Structure of Human Amylin Studied by Combined Hamiltonian and Temperature Replica Exchange Molecular Dynamics Simulations. Journal of Physical Chemistry B. 2010; 114:7071–7077.
30. Camargo DCR, Tripsianes K, Buday K, Franko A, Gobl C, Hartlmuller C, Sarkar R, Aichler M, Mettenleiter G, Schulz M, Boddrich A, Erck C, Martens H, Walch AK, Madl T, Wanker EE, Conrad M, de Angelis MH, Reif B. The redox environment triggers conformational changes and aggregation of hIAPP in Type II Diabetes. Scientific Reports. 2017; 7
31. Knowles TPJ, Waudby CA, Devlin GL, Cohen SIA, Aguzzi A, Vendruscolo M, Terentjev EM, Welland ME, Dobson CM. An Analytical Solution to the Kinetics of Breakable Filament Assembly. Science. 2009; 326:1533. [PubMed: 20007899]
32. Smith PES, Brender JR, Ramamoorthy A. Induction of Negative Curvature as a Mechanism of Cell Toxicity by Amyloidogenic Peptides: The Case of Islet Amyloid Polypeptide. Journal of the American Chemical Society. 2009; 131:4470–4478. [PubMed: 19278224]
33. Zhao J, Hu R, Sciacca MFM, Brender JR, Chen H, Ramamoorthy A, Zheng J. Non-selective ion channel activity of polymorphic human islet amyloid polypeptide (amylin) double channels. Physical Chemistry Chemical Physics. 2014; 16:2368–2377. [PubMed: 24352606]
34. Zhang M, Ren B, Liu Y, Liang G, Sun Y, Xu L, Zheng J. Membrane Interactions of hIAPP Monomer and Oligomer with Lipid Membranes by Molecular Dynamics Simulations. ACS Chemical Neuroscience. 2017; 8:1789–1800. [PubMed: 28585804]
35. Abedini A, Raleigh DP. Incorporation of Pseudoproline Derivatives Allows the Facile Synthesis of Human IAPP, a Highly Amyloidogenic and Aggregation-Prone Polypeptide. Organic Letters. 2005; 7:693–696. [PubMed: 15704927]
36. Marek P, Woys AM, Sutton K, Zanni MT, Raleigh DP. Efficient Microwave-Assisted Synthesis of Human Islet Amyloid Polypeptide Designed to Facilitate the Specific Incorporation of Labeled Amino Acids. Organic Letters. 2010; 12:4848–4851. [PubMed: 20931985]
37. Koo BW, Miranker AD. Contribution of the Intrinsic Disulfide to the Assembly Mechanism of Islet Amyloid. Protein science : a publication of the Protein Society. 2005; 14:231–239. [PubMed: 15576552]
38. Stewart JC. Colorimetric determination of phospholipids with ammonium ferrothiocyanate. Analytical Biochemistry. 1980; 104:10–14. [PubMed: 6892980]
39. Wong AG, Wu C, Hannaberry E, Watson MD, Shea J-E, Raleigh DP. Analysis of the Amyloidogenic Potential of Pufferfish (Takifugu rubripes) Islet Amyloid Polypeptide Highlights the Limitations of Thioflavin-T Assays and the Difficulties in Defining Amyloidogenicity. Biochemistry. 2016; 55:510–518. [PubMed: 26694855]
40. Tu L-H, Raleigh DP. Role of Aromatic Interactions in Amyloid Formation by Islet Amyloid Polypeptide. Biochemistry. 2013; 52:333–342. [PubMed: 23256729]
41. Marek PJ, Patsalo V, Green DF, Raleigh DP. Ionic Strength Effects on Amyloid Formation by Amylin Are a Complicated Interplay among Debye Screening, Ion Selectivity, and Hofmeister Effects. Biochemistry. 2012; 51:8478–8490. [PubMed: 23016872]
42. Trikha S, Jeremic AM. Clustering and Internalization of Toxic Amylin Oligomers in Pancreatic Cells Require Plasma Membrane Cholesterol. Journal of Biological Chemistry. 2011; 286:36086–36097. [PubMed: 21865171]
43. Caillon L, Duma L, Lequin O, Khemtemourian L. Cholesterol modulates the interaction of the islet amyloid polypeptide with membranes. Molecular Membrane Biology. 2014; 31:239–249. [PubMed: 25495656]
44. Zhang X, StClair JR, London E, Raleigh DP. Islet Amyloid Polypeptide Membrane Interactions: Effects of Membrane Composition. Biochemistry. 2017; 56:376–390. [PubMed: 28054763]
45. Cao P, Abedini A, Wang H, Tu L-H, Zhang X, Schmidt AM, Raleigh DP. Islet amyloid polypeptide toxicity and membrane interactions. Proceedings of the National Academy of Sciences. 2013; 110:19279–19284.

46. Sciacca Michele FM, Lolicato F, Di Mauro G, Milardi D, D'Urso L, Satriano C, Ramamoorthy A, La Rosa C. The Role of Cholesterol in Driving IAPP-Membrane Interactions. Biophysical Journal. 2016; 111:140–151. [PubMed: 27410742]
47. Cao P, Tu LH, Abedini A, Levsh O, Akter R, Patsalo V, Schmidt AM, Raleigh DP. Sensitivity of Amyloid Formation by Human Islet Amyloid Polypeptide to Mutations at Residue 20. Journal of Molecular Biology. 2012; 421:282–295. [PubMed: 22206987]
48. Hong D-P, Hoshino M, Kuboi R, Goto Y. Clustering of Fluorine-Substituted Alcohols as a Factor Responsible for Their Marked Effects on Proteins and Peptides. Journal of the American Chemical Society. 1999; 121:8427–8433.
49. Gilead S, Wolfenson H, Gazit E. Molecular Mapping of the Recognition Interface between the Islet Amyloid Polypeptide and Insulin. Angewandte Chemie International Edition. 2006; 45:6476–6480. [PubMed: 16960910]
50. Andreetto E, Yan LM, Tatarek-Nossol M, Velkova A, Frank R, Kapurniotu A. Identification of Hot Regions of the Aβ–IAPP Interaction Interface as High-Affinity Binding Sites in both Cross- and Self-Association. Angewandte Chemie International Edition. 2010; 49:3081–3085. [PubMed: 20309983]
51. Munoz V, Serrano L. Elucidating the folding problem of helical peptides using empirical parameters. Nat Struct Mol Biol. 1994; 1:399–409.
52. Abedini A, Raleigh DP. A critical assessment of the role of helical intermediates in amyloid formation by natively unfolded proteins and polypeptides. Protein Engineering, Design and Selection. 2009; 22:453–459.
53. Andisheh A, Daniel PR. A role for helical intermediates in amyloid formation by natively unfolded polypeptides? Physical Biology. 2009; 6:015005. [PubMed: 19208933]
54. Ilitchev AI, Giammona MJ, Do TD, Wong AG, Buratto SK, Shea JE, Raleigh DP, Bowers MT. Human Islet Amyloid Polypeptide N-Terminus Fragment Self-Assembly: Effect of Conserved Disulfide Bond on Aggregation Propensity. Journal of the American Society for Mass Spectrometry. 2016; 27:1010–1018. [PubMed: 26894887]
55. Apostolidou M, Jayasinghe SA, Langen R. Structure of α-Helical Membrane-bound Human Islet Amyloid Polypeptide and Its Implications for Membrane-mediated Misfolding. Journal of Biological Chemistry. 2008; 283:17205–17210. [PubMed: 18442979]

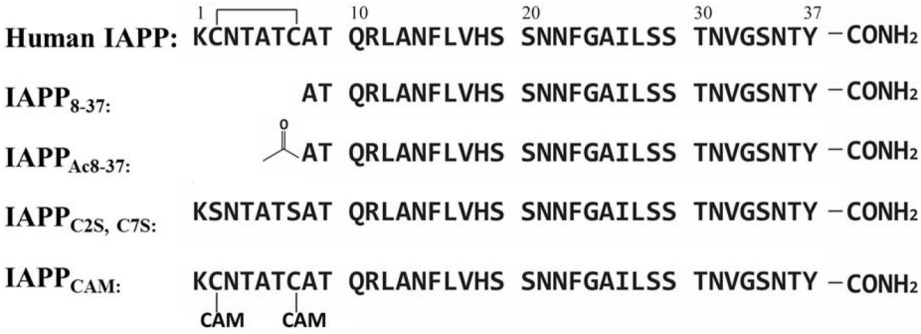

Figure 1.

Primary sequences of human IAPP, $IAPP_{C2S,\ C7S}$, $IAPP_{CAM}$, $IAPP_{8\text{-}37}$, and $IAPP_{Ac8\text{-}37}$. Both of the cysteine residues in $IAPP_{CAM}$ are blocked by a carboxyamidomethyl (CAM) protecting group. All peptides have an amidated C-terminus.

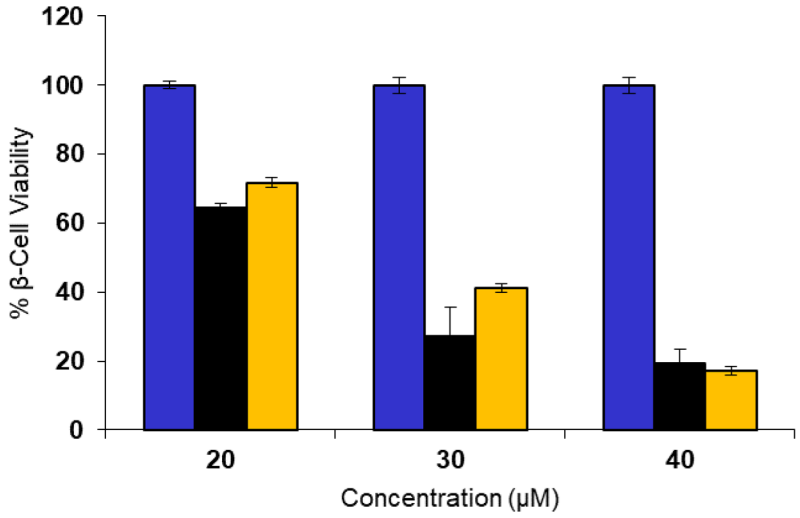

Figure 2.

$IAPP_{C2S, C7S}$ is toxic to INS-1 β-cells. Cell viability after treatment with hIAPP or $IAPP_{C2S, C7S}$, as determined by Alamar Blue reduction assays are shown. hIAPP (black), $IAPP_{C2S, C7S}$ (orange) and untreated cells (blue). Peptide was added at 20, 30, and 40μM concentrations to cultured INS-1 β-cells and incubated for 24 hours.

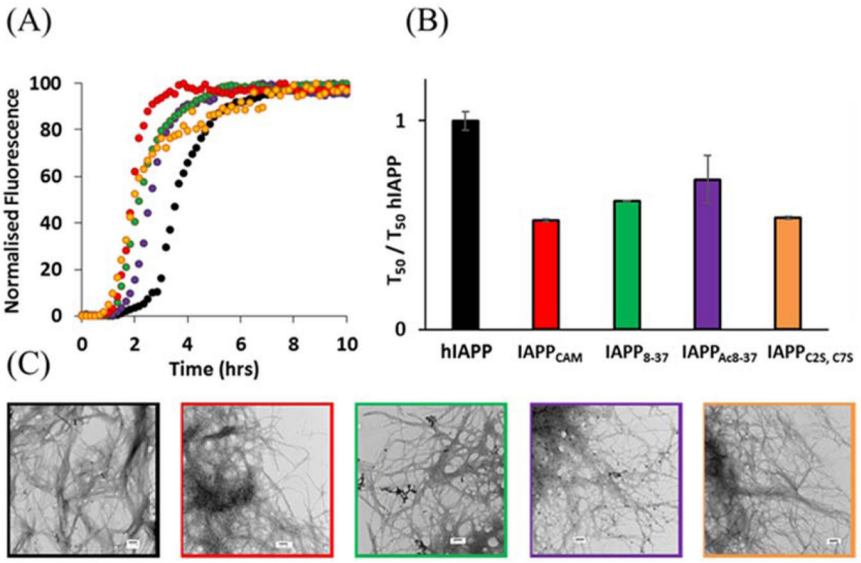

Figure 3.

Amyloid formation by hIAPP and disulfide-free variants in PBS (10mM sodium phosphate, 140mM KCl pH 7.4). (A) Time dependence of normalized thioflavin-T fluorescence for hIAPP (black), $IAPP_{CAM}$ (red), $IAPP_{8-37}$ (green), $IAPP_{Ac8-37}$ (purple) and $IAPP_{C2S, C7S}$ (orange). (B) T_{50} Values of disulfide free variants normalized with respect to the T_{50} of hIAPP. (C) TEM images of hIAPP (black) $IAPP_{CAM}$ (red) $IAPP_{8-37}$ (green) $IAPP_{Ac8-37}$ (purple) and $IAPP_{C2S, C7S}$ (orange). Aliquots were removed after 24 hours. Experiments were conducted with 16 μM peptide, 32 μM thioflavin-T at 25 °C in PBS at pH 7.4. Scale bars represent 100 nm.

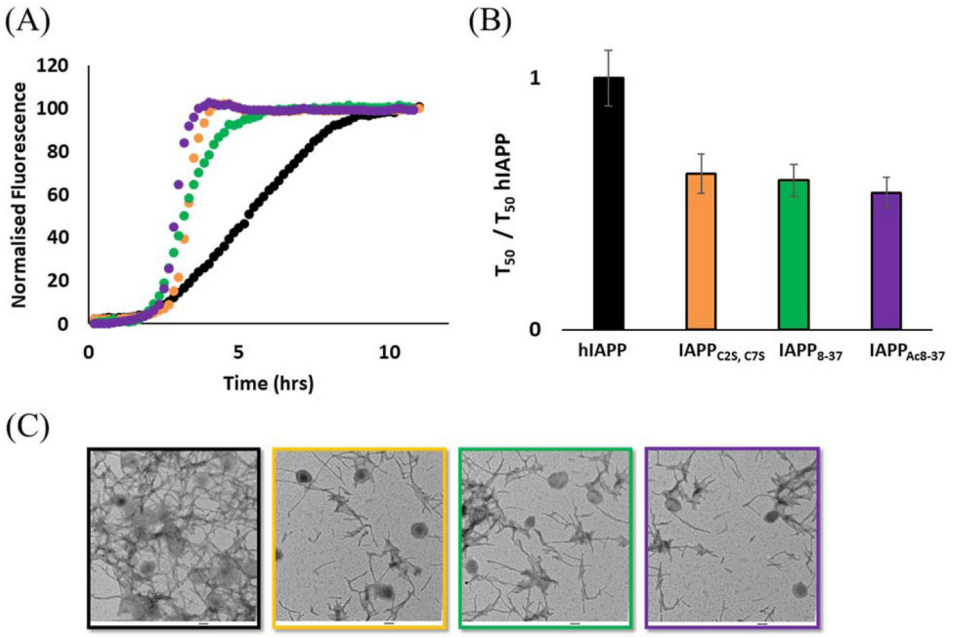

Figure 4.

Amyloid formation by wild type and disulfide-free variants of hIAPP in the presence of LUVs containing 25 mol% POPS and 75 mol% POPC. (A) Normalized fluorescence monitored by thioflavin-T assays for WT (black), $IAPP_{8-37}$ (green), $IAPP_{Ac8-37}$ (purple) and $IAPP_{C2S, C7S}$ (orange). (B) T_{50} Values of disulfide free variants normalized with respect to the T_{50} of WT. (C) TEM images of WT (black) $IAPP_{8-37}$ (green) $IAPP_{Ac8-37}$ (purple) and $IAPP_{C2S, C7S}$ (orange). Experiments were conducted in 20 mM Tris·HCl, 100 mM NaCl, pH 7.4 at 25 °C with 400 μM lipid and 20 μM peptide. Scale bars represent 100 nm.

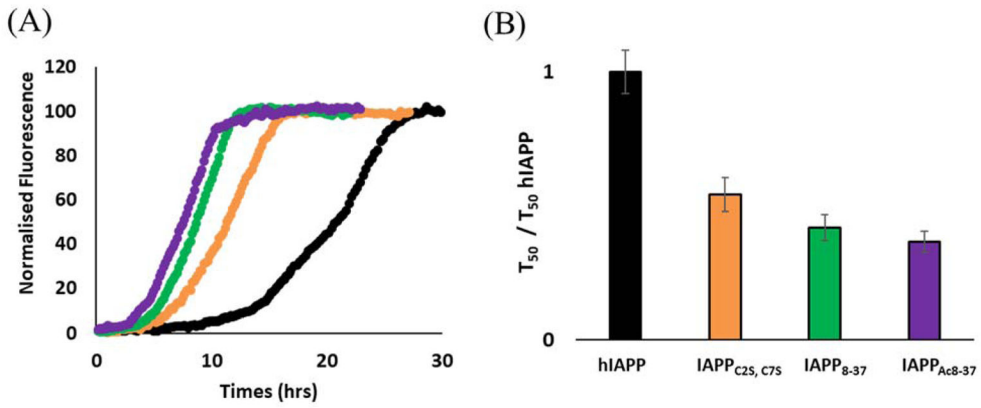

Figure 5.

Amyloid formation by wild type and disulfide-free variants in the presence of hIAPP of LUVs containing 40 mol% cholesterol, 10 mol% POPS and 50 mol% POPC. (A) Normalized Fluorescence monitored by thioflavin-T assay for WT (black), $IAPP_{8-37}$ (green), $IAPP_{Ac8-37}$ (purple) and $IAPP_{C2S, C7S}$ (orange). (B) T_{50} Values of disulfide free variants normalized with respect to the T_{50} of WT. Experiments were conducted in 20 mM Tris·HCl, 100 mM NaCl, pH 7.4 at 25 °C with 400 μM lipid and 20 μM peptide.

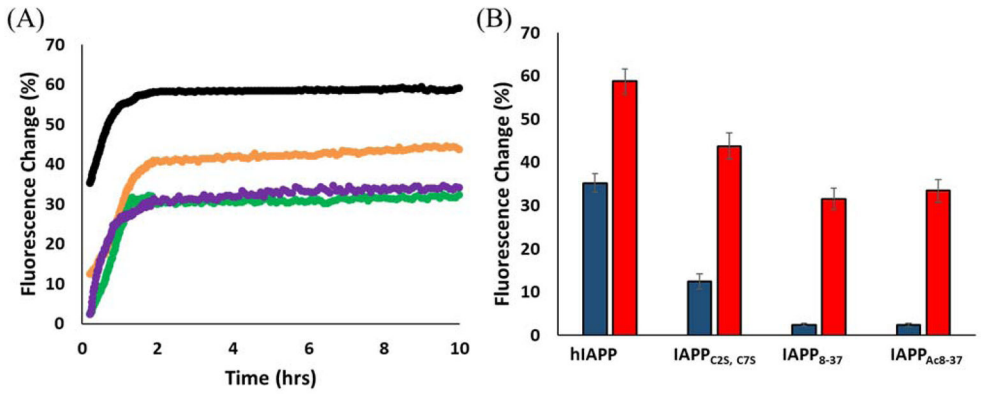

Figure 6.

Leakage induced by wild type and disulfide-free variants of hIAPP WT and disulfide-free variants in the presence of LUVs containing 25 mol% POPS and 75 mol% POPC. (A) Time course of the change in fluorescence (%) monitored by carboxyfluorescein assays for WT (black), $IAPP_{8-37}$ (green), $IAPP_{Ac8-37}$ (purple) and $IAPP_{C2S,\ C7S}$ (orange). (B) % leakage after ten minutes incubation (blue) and after incubation in the presence of LUV's for a time sufficient for each peptide to form amyloid (red). Experiments were conducted in 20 mM Tris·HCl, 100 mM NaCl, pH 7.4 at 25 °C with 400 μM lipid and 20 μM peptide.

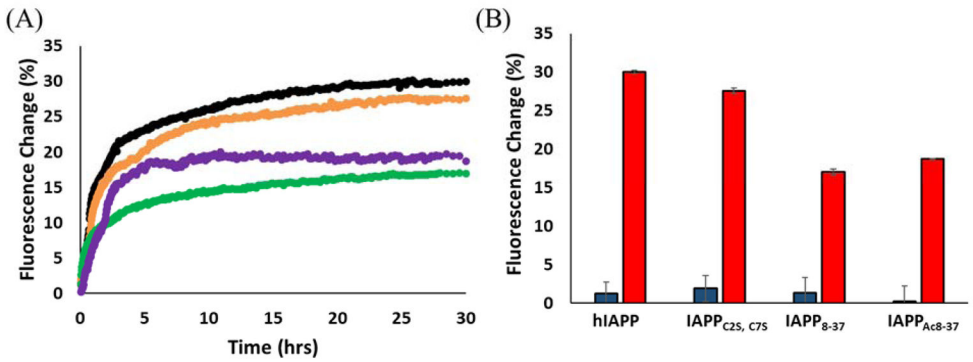

Figure 7.

Leakage induced by wild type and disulfide-free variants of hIAPP WT and disulfide-free variants in the presence of LUVs containing 40 mol% cholesterol, 10 mol% POPS and 50 mol% POPC. (A) Time course of the change in fluorescence monitored by carboxyfluorescein assay for WT (black), IAPP$_{8-37}$ (green), IAPP$_{Ac8-37}$ (purple) and IAPP$_{C2S, C7S}$ (orange). (B) % leakage after ten minutes incubation (blue) and after incubation in the presence of LUV's for a time sufficient for each peptide to form amyloid (red). Experiments were conducted in 20 mM Tris·HCl, 100 mM NaCl, pH 7.4 at 25 °C with 400 μM lipid and 20 μM peptide.